Electronic Supplementary Material (ESI) for Environmental Science: Nano.

Supporting Information

For

Nanoscale Imaging of Simultaneous Occlusion of Nanoplastics and Glyphosate within Soil Minerals

Jialin Chi,[1] Yafei Yin,[1] Wenjun Zhang,[1] Christine V. Putnis,[2,3] and Lijun Wang[*,1]

[1]College of Resources and Environment, Huazhong Agricultural University, Wuhan 430070, China

[2]Institut für Mineralogie, University of Münster, 48149 Münster, Germany

[3]School of Molecular and Life Science, Curtin University, 6845 Perth, Australia

SI Tables (1-7)

SI Figures (1-24)

SI References

Table S1. Supersaturated solution conditions of calcite for the experiments.

Experiments	σ	Concentration (mM)			Additives	pH
		$CaCl_2$	$K_2C_2O_4$	NaCl		
Adsorption	0.274	0.18	5.50	100	2.5 mg/L PS + 0, 0.025, 0.1, 0.25 mg/L PMG; 2.5 mg/L PS-COOH + 0, 0.025, 0.1, 0.25 mg/L PMG; 2.5 mg/L PS-HSO_3 + 0, 0.025, 0.1, 0.25 mg/L PMG; 2.5 mg/L NH_2 + 0, 0.025, 0.1, 0.25 mg/L PMG	8.3
Occlusion	1.196	0.30	9.00	100	0	8.3
Growth of hillocks	0.826	0.245	7.45	100	0.025, 0.25, 2.5 mg/L PS; 0.025, 0.25, 2.5 mg/L PS-COOH; 0.025, 0.25, 2.5 mg/L PS-HSO_3; .025, 0.25, 2.5 mg/L PS-NH_2; 2.5 mg/LPS + 0, 0.025, 0.1, 0.25 mg/L PMG; 2.5 mg/L PS-COOH + 0, 0.025, 0.1, 0.25 mg/L PMG; 2.5 mg/L PS-HSO_3 + 0, 0.025, 0.1, 0.25 mg/L PMG; 2.5 mg/L NH_2 + 0, 0.025, 0.1, 0.25 mg/L PMG	8.3
	1.030	0.275	8.25	100		8.3
	1.196	0.30	9.00	100		8.3
DFS	0.274	0.18	5.50	100	0, 0.025, 0.1, 0.25 mg/L	8.3

Table S2. Solution compositions of cell culture medium.

Component	Concentration (mg/L)	Component	Concentration (mg/L)
$CaCl_2 \cdot 2H_2O$	440	$FeSO_4 \cdot 7H_2O$	27.85
KH_2PO_4	170	Na_2EDTA	37.25
$MgSO_4 \cdot 7H_2O$	370	2,4-D	1.0
KCl	2940	Myo-Inositol	100
KI	0.83	Thiamine Hydrochloride	0.5
$CoCl_2 \cdot 6H_2O$	0.025	Glycine	75
H_3BO_3	6.2	L-Glutamine	877
$Na_2MoO_4 \cdot 2H_2O$	0.25	L-Aspartic acid	266
$MnSO_4 \cdot 4H_2O$	22.3	L-Arginine	228
$CuSO_4 \cdot 5H_2O$	0.025	Sucrose	30,000
$ZnSO_4 \cdot 7H_2O$	8.6	pH	5.6

Table S3. Raman shifts (cm^{-1}) of PSFG, PMG, calcite and iron hydroxides.

Composition	Wavenumber (cm^{-1})	Assignments
PS[1]	1001	Aromatic CC stretching
	1450	CH bending
	1598,1613	Aromatic ring quadrant stretching
PS-COOH[2]	1551	COH stretching
PS-HSO_3[3]	1435	HSO_3 asymmetric stretching
PS-NH_2[4]	1531	NH bending
PMG[5]	1551	COH stretching
	1714	CO asymmetric stretching
Calcite[6]	1086	CO symmetric stretching
Iron hydroxide[7]	290	Fe-O symmetric bending
	412	Fe-O symmetric stretching
	498	Fe-O symmetric bending
	607	Fe-O symmetric bending

Table S4. The growth of calcite hillocks in the presence of different concentrations of PSFG at σ = 1.196.

Experimental Condition	v_+ (nm/s)	v_- (nm/s)	v_m (nm/s)	v_+/v_- (nm/s)	Φ (°)
CK	7.56 ± 0.27	3.28 ± 0.13	10.85 ± 0.20	2.30 ± 0.15	146.8 ± 2.3
0.025mg/L PS	6.96 ± 0.19	3.02 ± 0.24	9.99 ± 0.22	2.30 ± 0.11	144.9 ± 3.1
0.25mg/L PS	6.64 ± 0.25	2.86 ± 0.18	9.51 ± 0.21	2.31 ± 0.16	147.8 ± 2.7
2.5mg/L PS	6.25 ± 0.26	2.71 ± 0.16	8.97 ± 0.23	2.30 ± 0.31	145.1 ± 1.8
0.025mg/L PS-COOH	6.38 ± 0.24	2.73 ± 0.11	9.12 ± 0.26	2.33 ± 0.23	144.5 ± 3.1
0.25mg/L PS-COOH	6.02 ± 0.31	2.58 ± 0.26	8.61 ± 0.31	2.33 ± 0.19	143.2 ± 2.6
2.5mg/L PS-COOH	5.59 ± 0.21	2.33 ± 0.16	7.92 ± 0.37	2.40 ± 0.38	142.6 ± 3.8
0.025mg/L PS-HSO_3	6.66 ± 0.35	2.82 ± 0.19	10.85 ± 0.20	2.30 ± 0.15	146.8 ± 2.3
0.25mg/L PS-HSO_3	6.19 ± 0.26	2.62 ± 0.17	8.81 ± 0.31	2.36 ± 0.28	150.3 ± 3.6
2.5mg/L PS-HSO_3	5.71 ± 0.29	2.38 ± 0.14	8.10 ± 0.15	2.40 ± 0.41	152.3 ± 2.9
0.025mg/L PS-NH_2	6.94 ± 0.25	2.88 ± 0.16	9.82 ± 0.30	2.41 ± 0.14	152.8 ± 4.1
0.25mg/L PS-NH_2	6.38 ± 0.23	2.67 ± 0.13	9.06 ± 0.33	2.39 ± 0.16	150.7 ± 4.6
2.5mg/L PS-NH_2	6.06 ± 017	2.56 ± 0.09	8.62 ± 0.25	2.36 ± 0.27	148.5 ± 3.6

Table S5. The growth of calcite hillocks in the presence of 2.5 mg/L PSFG mixed with different concentrations of PMG at σ = 1.196.

Experimental Condition	v_+ (nm/s)	v_- (nm/s)	v_m (nm/s)	v_+/v_- (nm/s)	Φ (°)
CK	7.56 ± 0.27	3.28 ± 0.13	10.85 ± 0.20	2.30 ± 0.15	146.8 ± 2.3
2.5mg/L PS	6.25 ± 0.26	2.71 ± 0.16	8.97 ± 0.23	2.30 ± 0.31	145.1 ± 1.8
2.5mg/L PS-COOH	5.59 ± 0.21	2.33 ± 0.16	7.92 ± 0.37	2.40 ± 0.38	142.6 ± 3.8
2.5mg/L PS-HSO_3	5.71 ± 0.29	2.38 ± 0.14	8.10 ± 0.15	2.40 ± 0.41	152.3 ± 2.9
2.5mg/L PS-NH_2	6.06 ± 017	2.56 ± 0.09	8.62 ± 0.25	2.36 ± 0.27	148.5 ± 3.6
0.025 mg/L PMG	5.06 ± 0.36	2.17 ± 0.13	7.33 ± 0.26	2.22 ± 0.27	154.3 ± 3.8
2.5mg/L PS + 0.025 mg/L PMG	5.65 ± 0.33	2.53 ± 0.19	8.18 ± 0.23	2.23 ± 0.25	155.6 ± 4.0
2.5mg/L PS-COOH + 0.025 mg/L PMG	5.06 ± 0.36	2.27 ± 0.14	7.34 ± 0.31	2.22 ± 0.28	153.8 ± 3.2
2.5mg/L PS-HSO_3 + 0.025 mg/L PMG	5.24 ± 0.26	2.27 ± 0.19	7.52 ± 0.34	2.30 ± 0.41	154.7 ± 2.9
2.5mg/L PS-NH_2 + 0.025 mg/L PMG	5.76 ± 0.24	2.58 ± 0.16	8.34 ± 0.18	2.23 ± 0.22	157.6 ± 2.8
0.1 mg/ L PMG	4.60 ± 0.28	2.10 ± 0.14	6.69 ± 0.35	2.19 ± 0.26	158.3 ± 2.6
2.5mg/L PS + 0.1 mg/ L PMG	5.25 ± 0.34	2.41 ± 0.28	7.66 ± 0.27	2.18 ± 0.28	156.9 ± 3.3
2.5mg/L PS-COOH + 0.1 mg/ L PMG	4.62 ± 0.37	2.10 ± 0.15	6.73 ± 0.36	2.19 ± 0.36	158.8 ± 3.7
2.5mg/L PS-HSO_3 + 0.1 mg/ L PMG	4.83 ± 0.39	2.16 ± 0.17	7.00 ± 0.19	2.23 ± 0.39	160.2 ± 3.5
2.5mg/L PS-NH_2 + 0.25 mg/L PMG	5.42 ± 0.29	2.32 ± 0.16	7.74 ± 0.28	2.33 ± 0.36	161.3 ± 2.9
0.25 mg/L PMG	4.27 ± 0.31	2.08 ± 0.22	6.36 ± 0.26	2.05 ± 0.11	162.2 ± 4.6
2.5mg/L PS + 0.25 mg/L PMG	4.99 ± 0.36	2.29 ± 0.23	7.29 ± 0.37	2.17 ± 0.28	161.4 ± 3.9
2.5mg/L PS-COOH + 0.25 mg/L PMG	4.49 ± 0.27	2.08 ± 0.17	6.57 ± 0.28	2.15 ± 0.25	162.3 ± 4.2

2.5mg/L PS-HSO_3 + 0.25 mg/L PMG	4.62 ± 0.25	2.13 ± 0.18	6.76 ± 0.36	2.16 ± 0.34	163.1 ± 3.8
2.5mg/L PS-NH_2 + 0.25 mg/ L PMG	5.20 ± 0.16	2.32 ± 0.09	6.75 ± 0.19	2.23 ± 0.22	161.7 ± 3.5

Table S6. The growth of calcite hillocks in the presence of 2.5 mg/L PSFG mixed with 0.25 mg/L PMG at different supersaturated solutions.

Experimental Condition	v_+ (nm/s)	v_- (nm/s)	v_m (nm/s)	v_+/v_- (nm/s)	Φ (°)
		σ = 0.826			
CK	5.66 ± 0.13	2.66 ± 0.06	8.32 ± 0.15	2.12 ± 0.16	147.3 ± 3.2
0.25 mg/L PMG	3.08 ± 0.16	1.56 ± 0.11	4.64 ± 0.21	1.97 ± 0.23	147.3 ± 3.1
2.5mg/L PS + 0.25 mg/L PMG	3.69 ± 0.12	1.82 ± 0.09	5.51 ± 0.16	2.02 ± 0.22	160.7 ± 4.2
2.5mg/L PS-COOH + 0.25 mg/L PMG	3.35 ± 0.21	1.65 ± 0.13	5.08 ± 0.28	2.05 ± 0.32	159.5 ± 2.7
2.5mg/L PS-HSO_3 + 0.25 mg/L PMG	3.42 ± 0.23	1.66 ± 0.11	5.08 ± 0.28	2.05 ± 0.32	159.5 ± 2.7
2.5mg/L PS-NH_2 + 0.25 mg/ L PMG	3.83 ± 0.15	1.85 ± 0.13	5.69 ± 0.16	2.06 ± 0.11	160.6 ± 1.2
		σ = 1.030			
CK	6.70 ± 0.16	2.83 ± 0.08	9.53 ± 0.24	2.36 ± 0.11	150.2 ± 2.2
0.25 mg/L PMG	3.80 ± 0.14	1.69 ± 0.11	5.49 ± 0.23	2.24 ± 0.28	159.7 ± 3.5
2.5mg/L PS + 0.25 mg/L PMG	4.37 ± 0.23	1.93 ± 0.10	6.31 ± 0.26	2.26 ± 0.13	158.7 ± 2.7
2.5mg/L PS-COOH + 0.25 mg/L PMG	3.94 ± 0.22	1.69 ± 0.16	5.63 ± 0.35	2.32 ± 0.16	160.3 ± 2.6
2.5mg/L PS-HSO_3 + 0.25 mg/L PMG	4.06 ± 0.15	1.79 ± 0.06	5.85 ± 0.26	2.26 ± 0.21	161.2 ± 3.1
2.5mg/L PS-NH_2 + 0.25 mg/ L PMG	4.48 ± 0.19	1.86 ± 0.09	6.35 ± 0.25	2.40 ± 0.08	160.4 ± 2.5
		σ = 1.196			
CK	7.56 ± 0.27	3.28 ± 0.13	10.85 ± 0.20	2.30 ± 0.15	146.8 ± 2.3
0.25 mg/L PMG	4.27 ± 0.31	2.08 ± 0.22	6.36 ± 0.26	2.05 ± 0.11	162.2 ± 4.6
2.5mg/L PS + 0.25 mg/L PMG	4.99 ± 0.36	2.29 ± 0.23	7.29 ± 0.37	2.17 ± 0.28	161.4 ± 3.9

2.5mg/L PS-COOH + 0.25 mg/L PMG	4.49 ± 0.27	2.08 ± 0.17	6.57 ± 0.28	2.15 ± 0.25	162.3 ± 4.2
2.5mg/L PS-HSO_3 + 0.25 mg/L PMG	4.62 ± 0.25	2.13 ± 0.18	6.76 ± 0.36	2.16 ± 0.34	163.1 ± 3.8
2.5mg/L PS-NH_2 + 0.25 mg/ L PMG	5.20 ± 0.16	2.32 ± 0.09	6.75 ± 0.19	2.23 ± 0.22	161.7 ± 3.5

Table S7. The fitting parameters from DFS data.

Groups	PMG concentration (mg/L)	f_{eq} (pN)	x_t (Å)	$-\Delta G_b$ (kJ/mol)
CH_3	0	101.05 ± 13.07	1.40 ± 0.02	17.08 ± 3.33
	0.025	145.35 ± 8.04	1.41 ± 0.02	23.36 ± 2.62
	0.1	168.13 ± 9.66	1.49 ± 0.01	27.97 ± 2.88
	0.25	191.39 ± 11.49	1.42 ± 0.03	30.00 ± 1.84
COO^-	0	453.75 ± 10.46	1.34 ± 0.06	63.67 ± 3.69
	0.025	513.45 ± 7.49	1.42 ± 0.04	75.76 ± 2.49
	0.1	580.41 ± 7.89	1.39 ± 0.02	84.61 ± 1.79
	0.25	652.96 ± 8.62	1.39 ± 0.02	90.85 ± 6.72
HSO_3^-	0	284.99 ± 13.36	1.32 ± 0.01	40.54 ± 4.22
	0.025	361.22 ± 11.69	1.42 ± 0.03	54.24 ± 3.23
	0.1	427.86 ± 9.81	1.47 ± 0.06	65.75 ± 2.84
	0.25	472.99 ± 8.48	1.38 ± 0.03	68.05 ± 2.46
NH_3^+	0	93.3 ± 10.08	1.38 ± 0.03	15.80 ± 3.59
	0.025	170.38 ± 8.20	1.46 ± 0.10	27.85 ± 2.26
	0.1	280.8 ± 7.97	1.42 ± 0.04	42.87 ± 3.49
	0.25	346.92 ± 9.94	1.38 ± 0.05	51.02 ± 3.

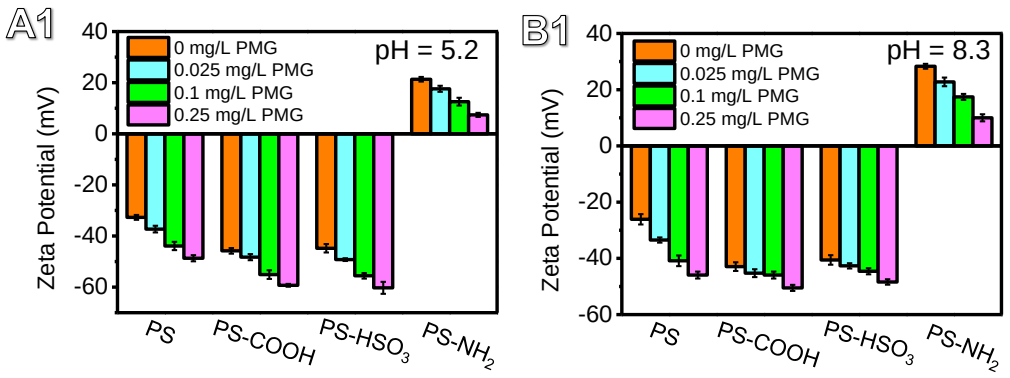

Figure S1. Aqueous zeta potentials obtained in solutions of 2.5 mg/L PSFG mixed with varied concentrations of PMG at (A) pH = 5.2 and (B) pH = 8.3 (*IS* = 0.11 M).

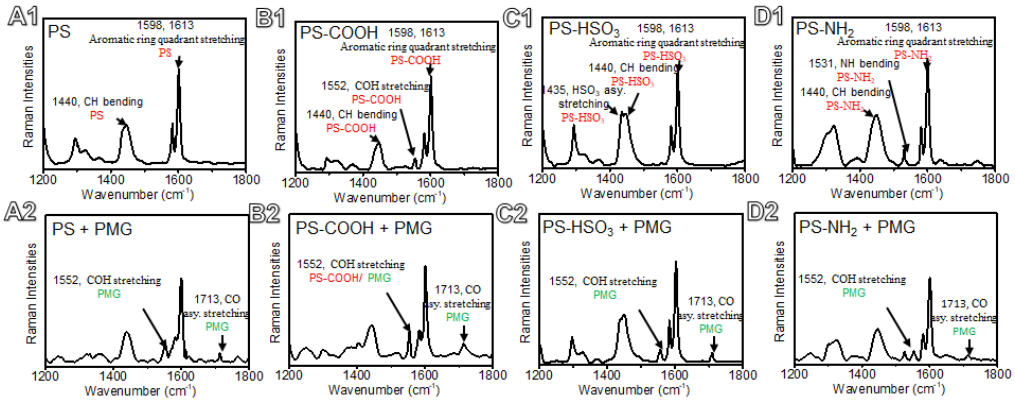

Figure S2. (A1-D1) Raman spectra of the 2.5 mg/L PSFG particles deposited on mica. PSFG showing the characteristic peaks of CH bending at 1440 cm^{-1} and aromatic ring quadrant stretching at 1598 cm^{-1}, COH stretching at 1551 cm^{-1}, the HSO_3 asymmetric stretching at 1435 cm^{-1}, and NH bending at 1531 cm^{-1}. (A2-D2) Raman spectra of the PSFG particles deposited on mica mixed with 0.25 mg/L PMG showing the characteristic peaks of COH stretching at 1552 cm^{-1} and CO asymmetric stretching at 1713 cm^{-1} for PMG.

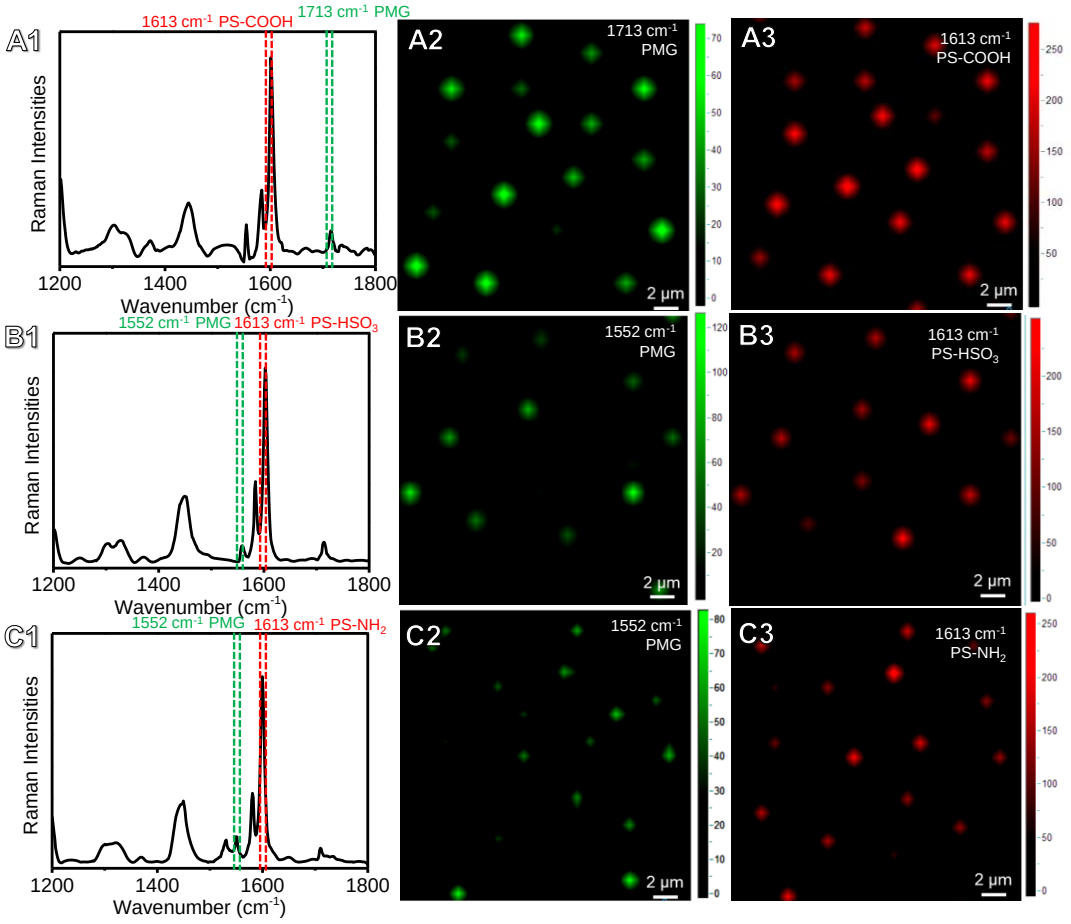

Figure S3. Raman mapping of 2.5 mg/L PMG and 0.25 mg/L PSFG at different characteristic peaks indicating the PSFG-PMG interactions.

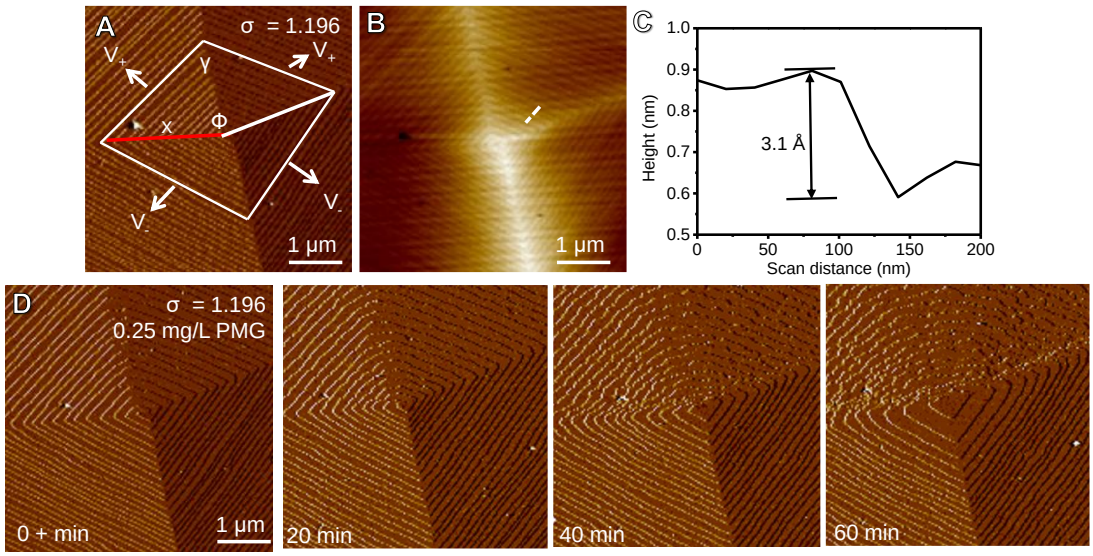

Figure S4. (A) AFM deflection and (B) height images of the $(10\bar{1}4)$ cleavage surface of calcite, showing a rhombohedral spiral grown through monomolecular step movements with the (C) height of 3.1 Å along a white dashed line in (B) in a supersaturated solution at $\sigma = 1.196$ (pH = 8.3, $IS = 0.11$ M). (D) AFM deflection images of a calcite surface grown in a supersaturated solution ($\sigma = 1.196$, pH 8.3, $IS = 0.11$ M) in the presence of 0.25 mg/L PMG. The obtuse steps became rougher and the morphology of the calcite hillocks was transformed from rhombus to fan-shaped.

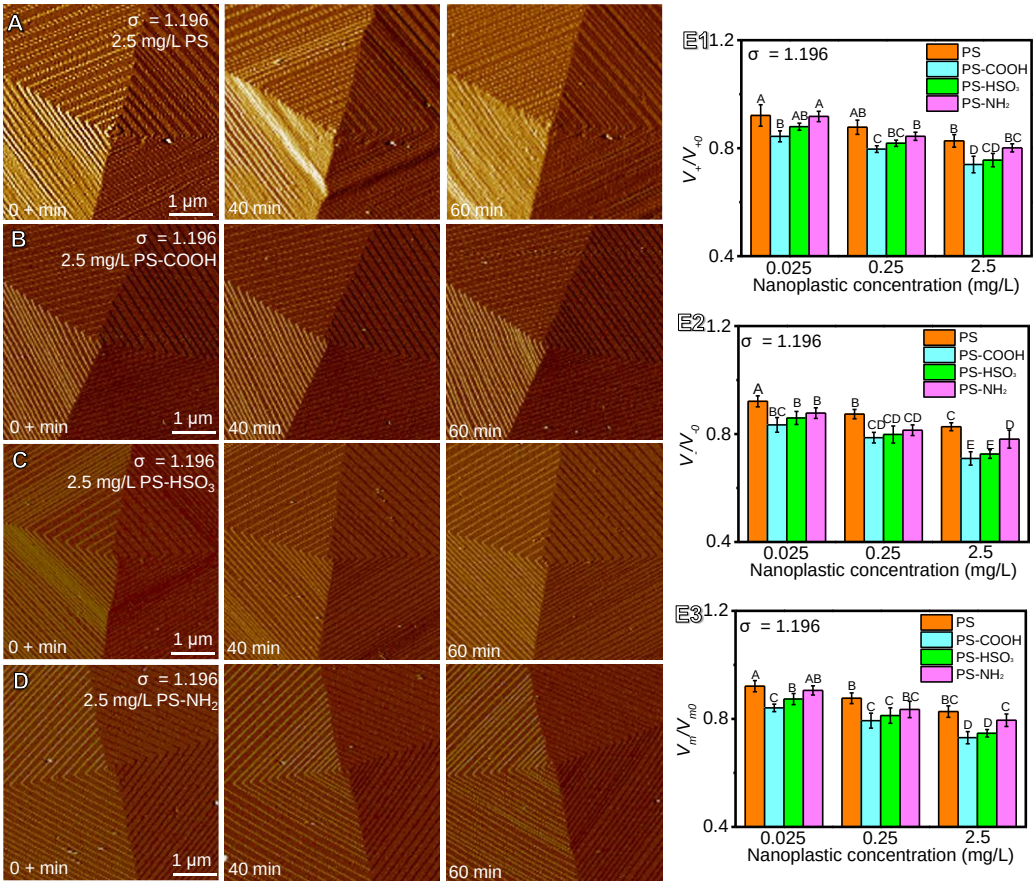

Figure S5. AFM deflection images of a calcite surface grown in a supersaturated solution (σ = 1.196, pH 8.3, I = 0.11 M) in the presence of (A) 2.5 mg/L PS, (B) 2.5 mg/L PS-COOH, (C) 2.5 mg/L PS-HSO_3, and (D) 2.5 mg/L PS-NH_2. Relative step movement velocities of (E1)v_+, (E2)v_- and (E3)v_m as a function of PSFG concentrations at σ = 1.196. Different uppercase letters indicate significant differences at $P < 0.01$.

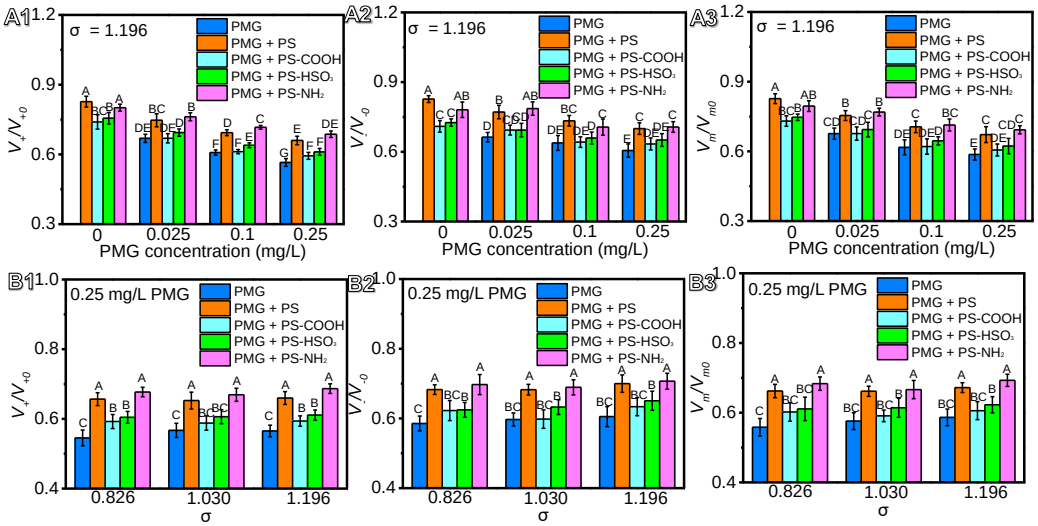

Figure S6. Relative step movement velocities of (A1) v_+, (A2) v_- and (A3) v_m in solutions containing 2.5 mg/L PSFG and varied concentrations of PMG at σ = 1.196 (pH = 8.3). Relative step movement velocities of (B1) v_+, (B2) v_- and (B3) v_m in solutions of 2.5 mg/L PSFG and 0.25 mg/mL PMG at different supersaturations (pH = 8.3). Different uppercase letters indicate significant differences at $P < 0.01$.

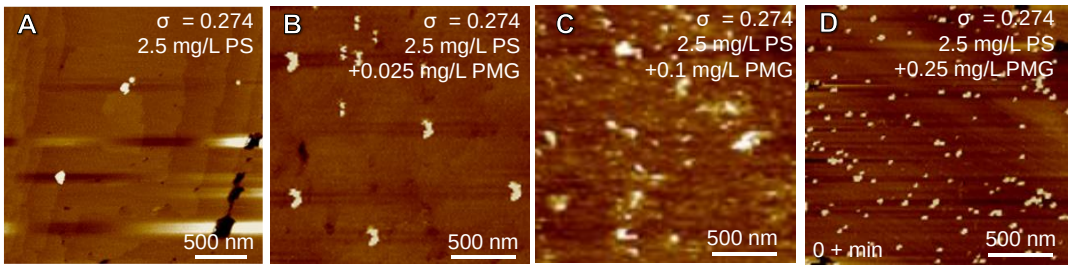

Figure S7. AFM height images of the adsorption of PS and PMG in calcite supersaturated solutions containing PS with varied concentrations of PMG (σ = 0.274, pH = 8.3) for 15 min prior to the occlusion process.

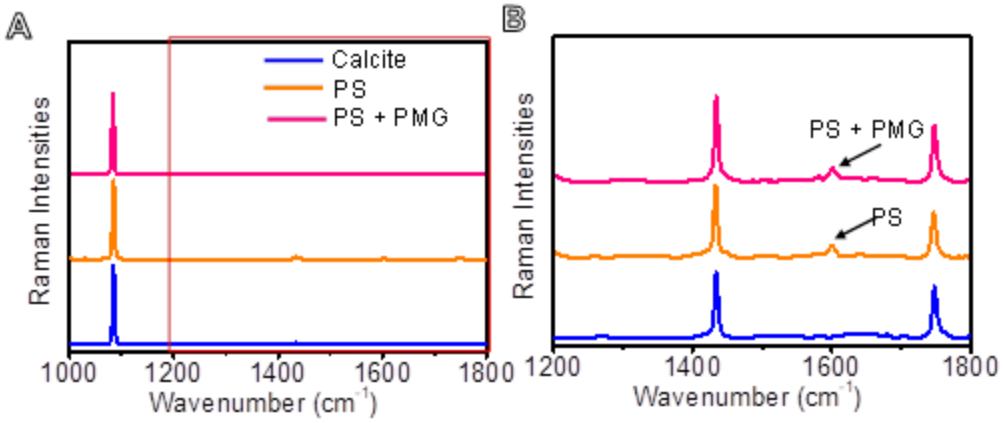

Figure S8. (A) Raman spectra after the adsorption and occlusion of 2.5 mg/L PS or 2.5 mg/L PS mixed with 0.25 mg/L PMG on calcite surfaces. (B) An enlargement of the marked range in (A) by a red square. The PS or PS + PMG signal are marked by the arrows.

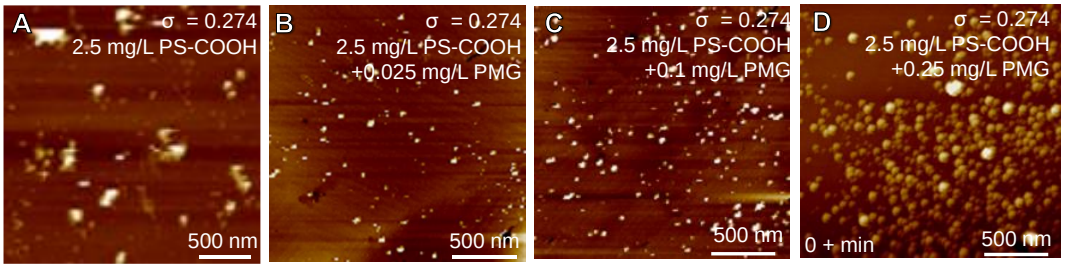

Figure S9. AFM height images of the adsorption of PS-COOH and PMG in calcite supersaturated solutions containing PS-COOH mixed with varied concentrations of PMG (σ = 0.274, pH = 8.3) for 15 min prior to the occlusion process.

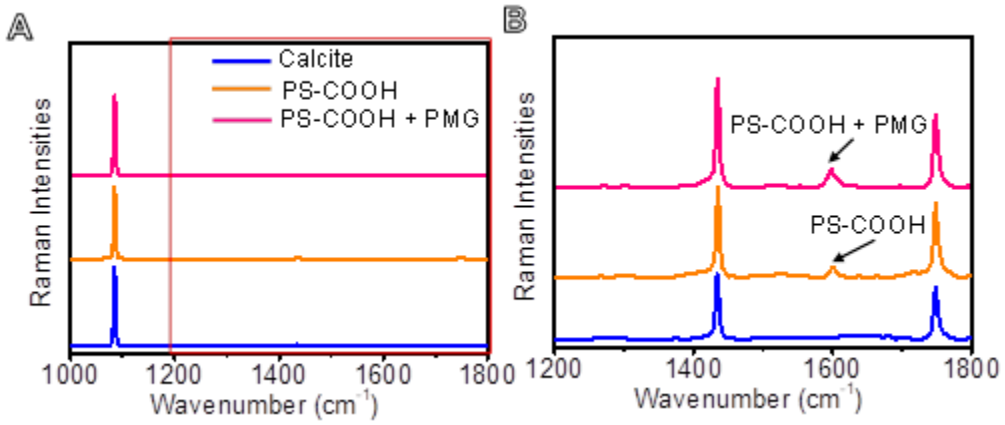

Figure S10. (A) Raman spectra after the adsorption and occlusion of 2.5 mg/L PS-COOH or 2.5 mg/L PS-COOH mixed with 0.25 mg/L PMG on calcite surfaces. (B) An enlargement of the marked range in (A) by a red square. The PS-COOH or PS-COOH + PMG signal is marked by the arrow.

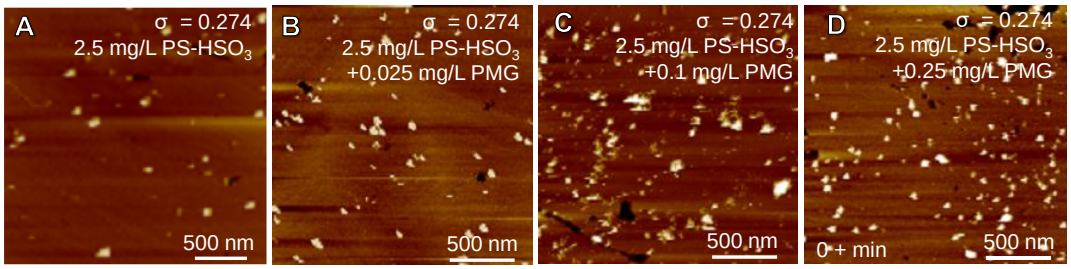

Figure S11. AFM height images of the adsorption of PS-HSO_3 and PMG in calcite supersaturated solutions containing PS-HSO_3 mixed with varied concentrations of PMG (σ = 0.274, pH = 8.3) for 15 min prior to the occlusion process.

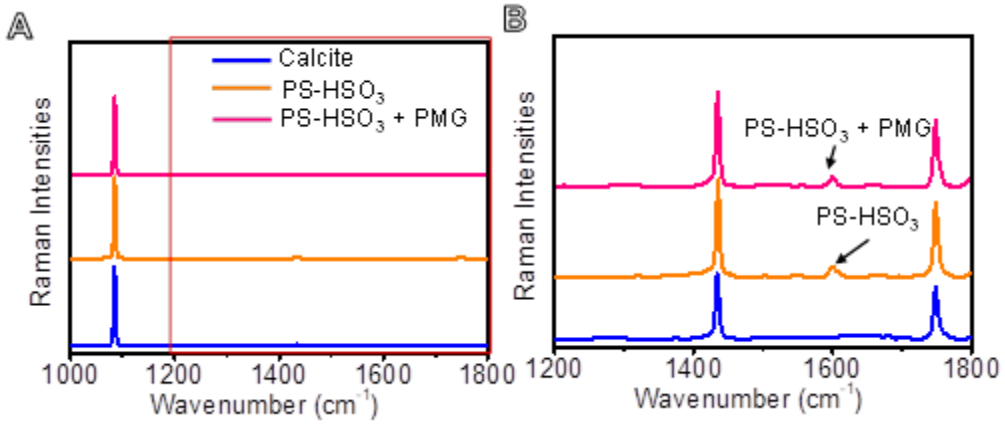

Figure S12. (A) Raman spectra after the adsorption and occlusion of 2.5 mg/L PS-HSO_3 or 2.5 mg/L PS-HSO_3 mixed with 0.25 mg/L PMG on calcite surfaces. (B) An enlargement of the marked range in (A) by a red square. The PS-HSO_3 or PS-HSO_3 + PMG signal is marked by the arrow.

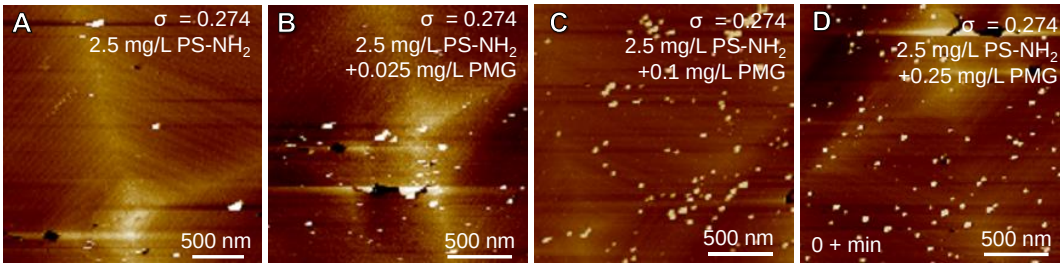

Figure S13. AFM height images of the adsorption of PS-NH_2 and PMG in calcite supersaturated solutions containing PS-NH_2 mixed with PMG at different concentrations (σ = 0.274, pH = 8.3) for 15 min prior to the occlusion process.

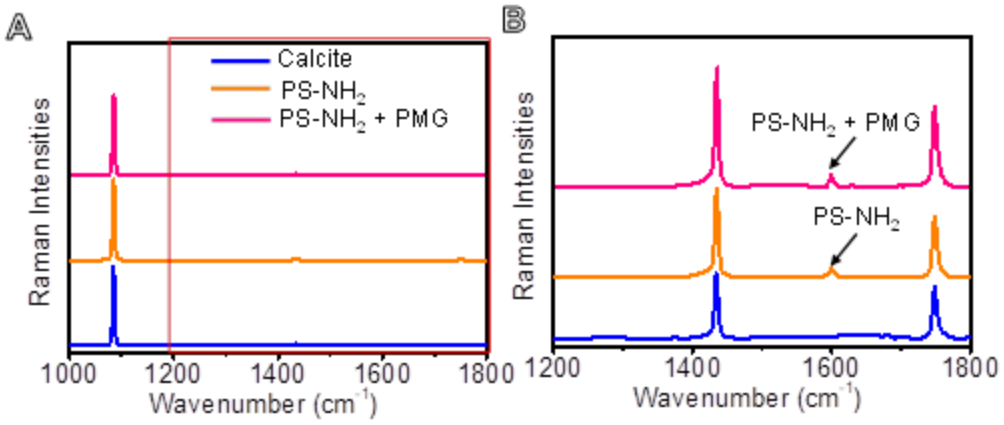

Figure S14. (A) Raman spectra after the adsorption and occlusion of 2.5 mg/L PS-NH_2 or 2.5 mg/L PS-NH_2 mixed with 0.25 mg/L PMG on calcite surfaces. (B) An enlargement of the marked range in (A) by a red square. The PS-NH_2 or PS-NH_2 + PMG signal is marked by the arrow.

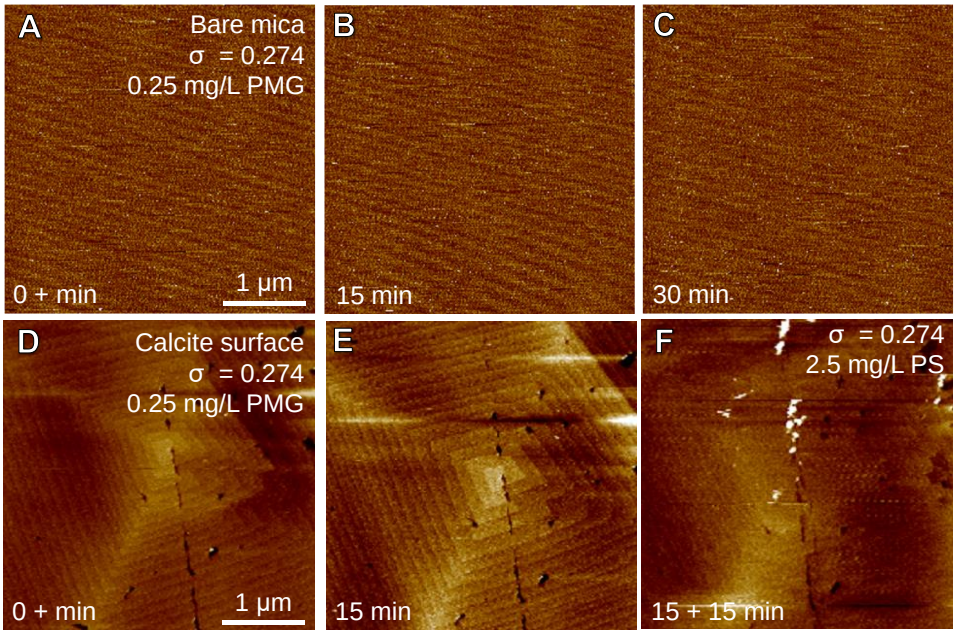

Figure S15. (A-C) Time sequence of AFM height images of calcite supersaturated solutions (σ = 0.274, pH 8.3) with 0.25 mg/L PMG on a mica surface. No particles deposited on the mica. (D, E) Time sequence of AFM height images of calcite grown in a supersaturated solution (σ = 0.274, pH 8.3) with 0.25 mg/L PMG on the calcite

surface showing that no particles deposited on the calcite. (F) AFM height images of the adsorption of PS particles on calcite grown in a supersaturated solution at σ = 0.274 containing 2.5 mg/L PS after mixture with PMG for 15 min. The adsorbed particle numbers were not changed significantly compared with the direct injection of PS.

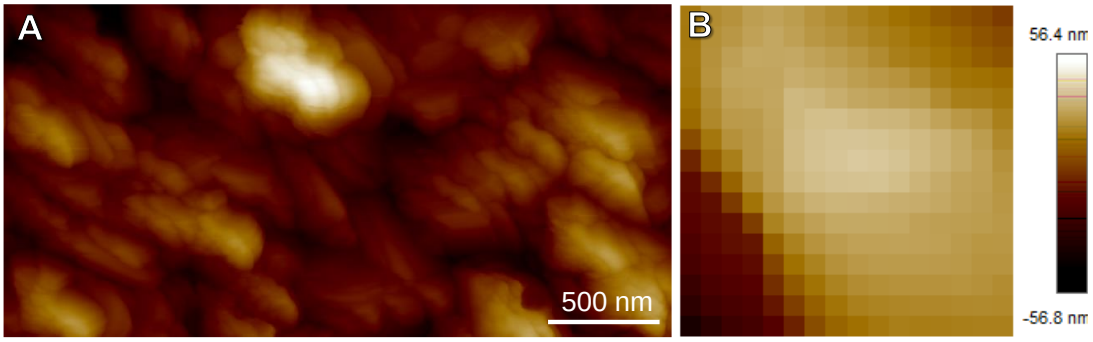

Figure S16. The corrected AFM tip radius of the functional group-modified AFM tips.

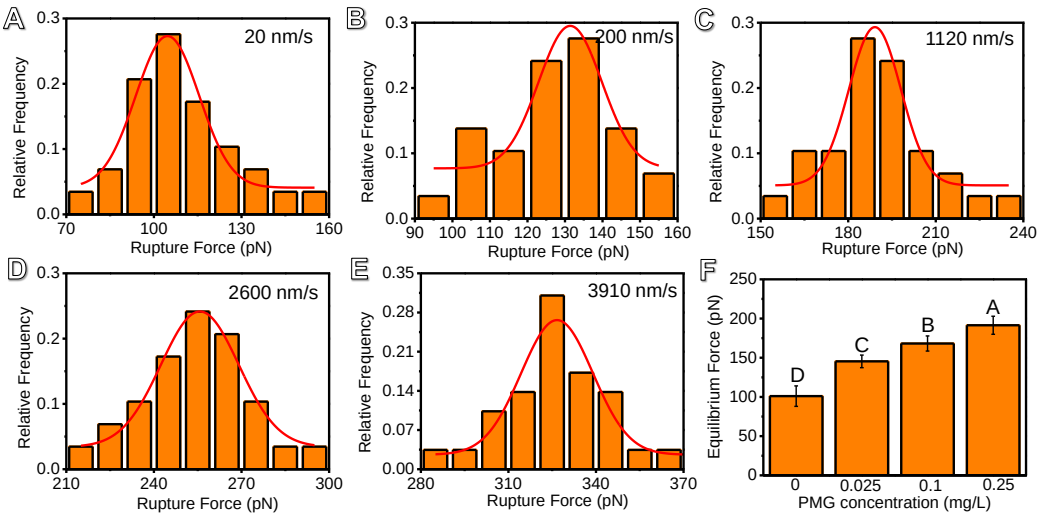

Figure S17. (A-E) The rupture forces between CH_3 groups and a calcite face at σ = 0.274 at different loading rates ranging from 20-3910 nm/s. (F) The equilibrium force between the CH_3 groups and calcite faces at different concentrations of PMG. Different uppercase letters indicate significant differences at $P < 0.01$.

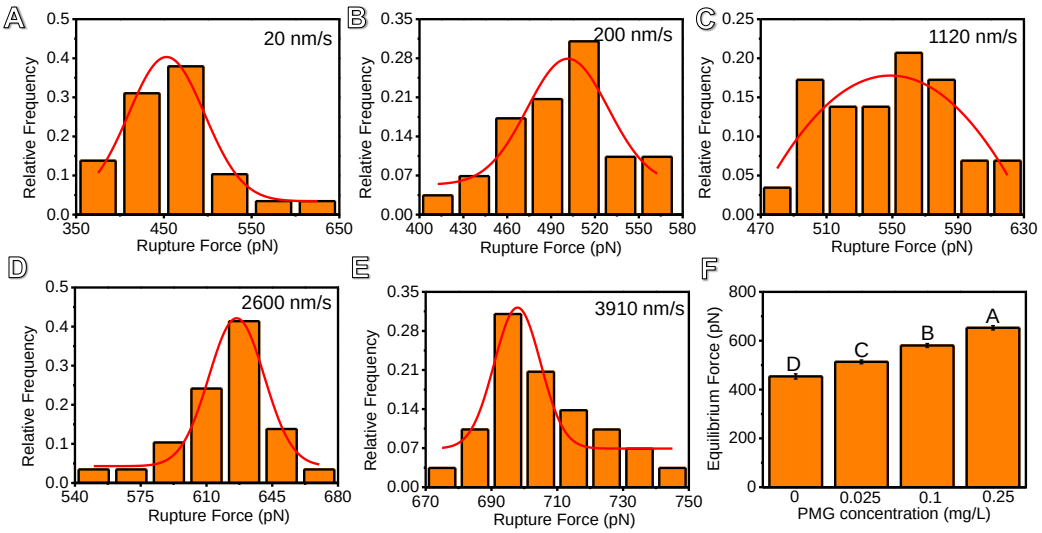

Figure S18. (A-E) The rupture forces between the COO^- groups and a calcite face at σ = 0.274 at different loading rates ranging from 20-3910 nm/s. (F) The equilibrium force between the COO^- groups and calcite faces at different concentrations of PMG. Different uppercase letters indicate significant differences at $P < 0.01$.

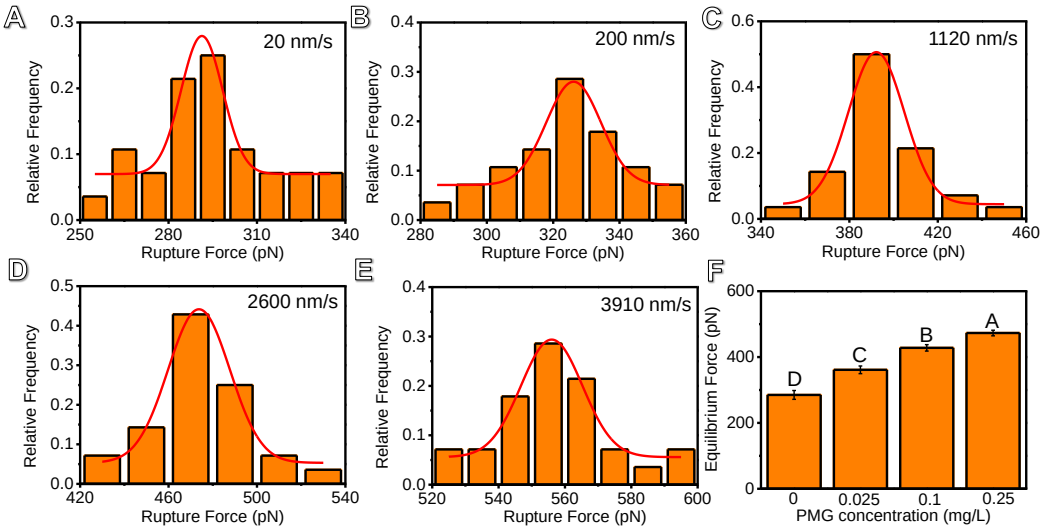

Figure S19. (A-E) The rupture forces between HSO_3^- groups and a calcite face at σ = 0.274 at different loading rates ranging from 20-3910 nm/s. (F) The equilibrium force

between the HSO_3^- groups and calcite faces at different concentrations of PMG. Different uppercase letters indicate significant differences at $P < 0.01$.

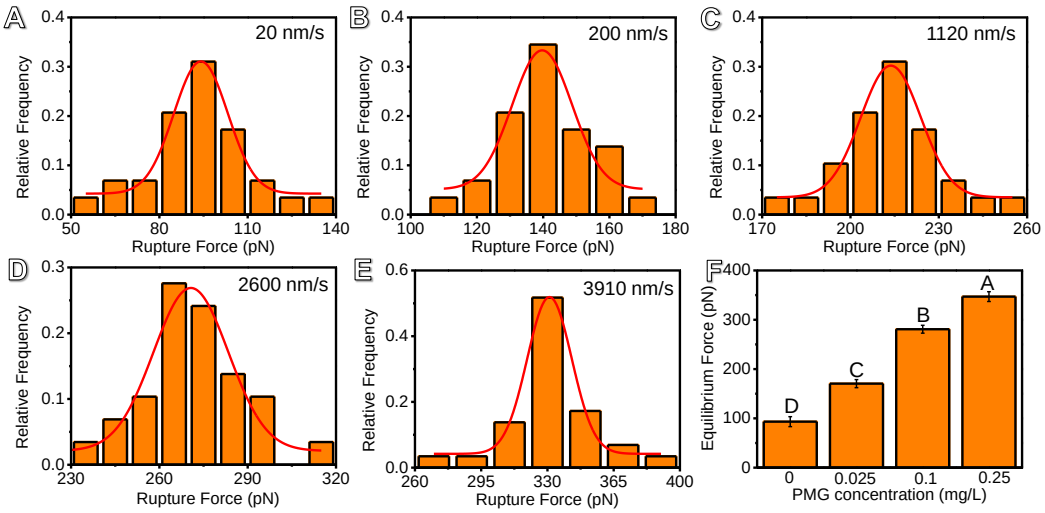

Figure S20. (A-E) The rupture forces between NH_3^+ groups and a calcite face at σ = 0.274 at different loading rates ranging from 20-3910 nm/s. (F) The equilibrium force between the NH_3^+ groups and calcite faces at different concentrations of PMG. Different uppercase letters indicate significant differences at $P < 0.01$.

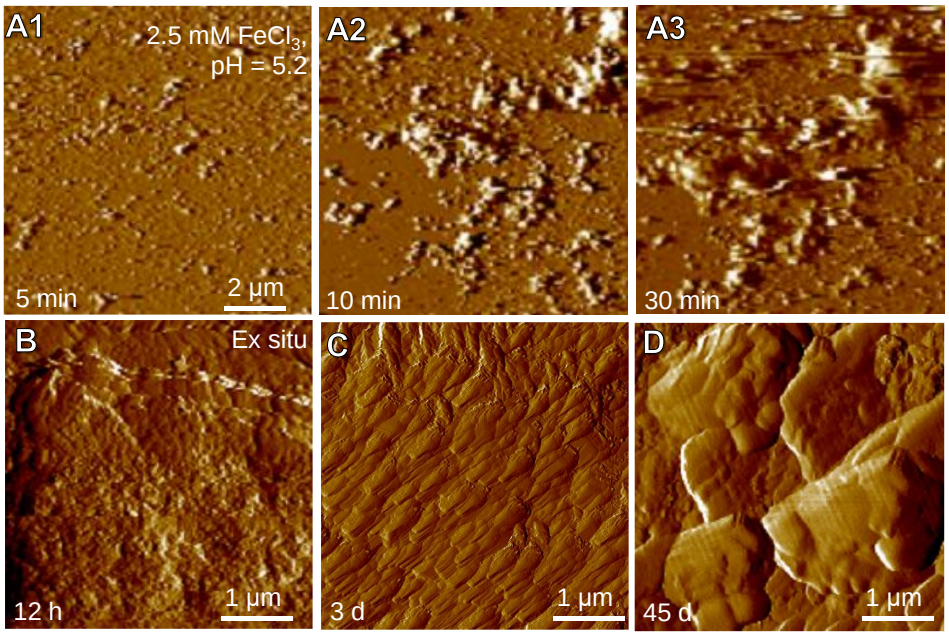

Figure S21. (A1-A3) Time sequence of AFM deflection images of the in situ nucleation and aggregation of iron hydroxide particles. Iron hydroxide deposited on (A1) mica and (A2, A3) the newly formed aggregated particles. (B-D) Ex situ AFM deflection imaging of the crystallization and phase transformation process of the iron hydroxide precipitates in solutions showing that certain crystalline faces appeared after 45 d of reactions.

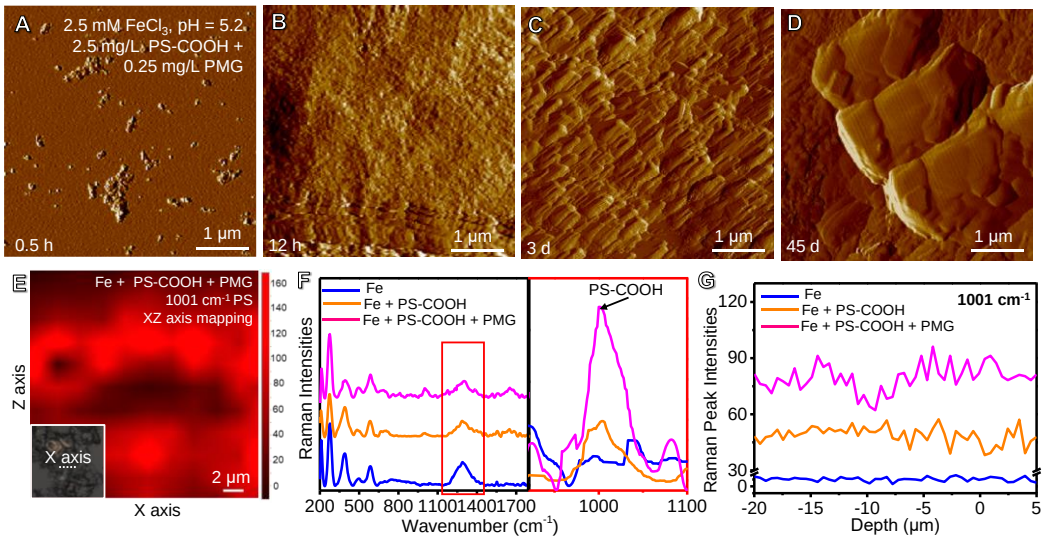

Figure S22. (A-D) Ex situ AFM deflection imaging of the crystallization and phase transformation process of iron hydroxide precipitates in solutions containing PS-COOH and PMG showing that certain crystalline faces appeared after 45 d of reactions. (E) Raman mapping (at 1001 cm^{-1}) of the XZ axis for the iron hydroxide precipitates containing PS-COOH and PMG after 120 h of reactions, indicating the PS-COOH was occluded within the crystals. (F) Raman spectra of iron hydroxide in the absence and presence of 2.5 mg/L PS-COOH or mixed 2.5 mg/L PS-COOH and 0.25 mg/L PMG. The PS-COOH signals were stronger for mixed PS-COOH and PMG than PS-COOH alone. (G) The z axis signal intensities (at 1001 cm^{-1}) of PS-COOH in the iron hydroxide in the presence of PS-COOH and PMG.

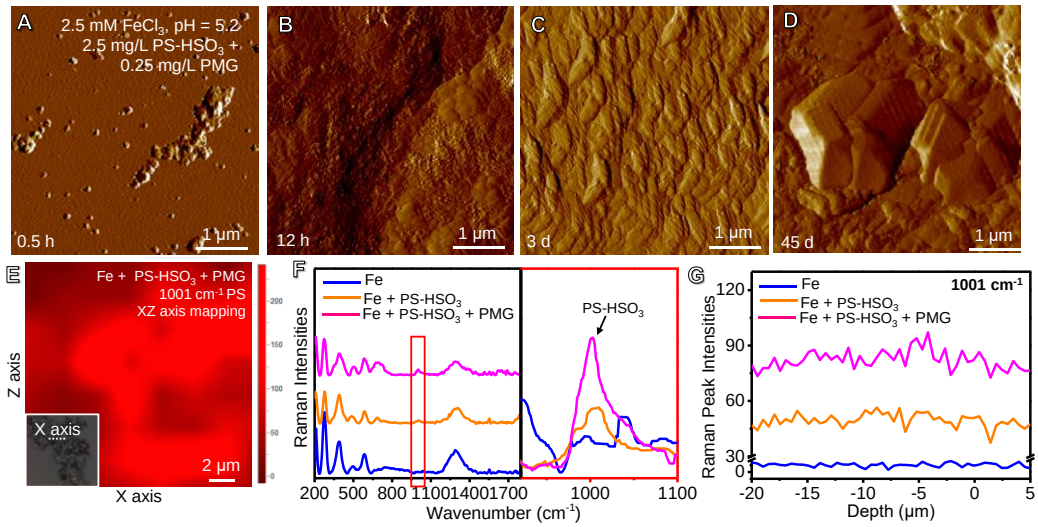

Figure S23. (A-D) Ex situ AFM deflection imaging of the crystallization and phase transformation process of iron hydroxide precipitates in solutions containing PS-HSO_3 and PMG showing that certain crystalline faces appeared after 45 d of reactions. (E) Raman mapping (at 1001 cm^{-1}) of the XZ axis for the iron hydroxide precipitates containing PS-HSO_3 and PMG after 120 h of reactions, indicating the PS-HSO_3 was occluded within the crystals. (F) Raman spectra of iron hydroxide in the absence and

presence of 2.5 mg/L PS-HSO_3 or mixed 2.5 mg/L PS-HSO_3 and 0.25 mg/L PMG. The PS-HSO_3 signals were stronger for mixed PS-HSO_3 and PMG than PS-HSO_3 alone. (G) The z axis signal intensities (at 1001 cm^{-1}) of PS-HSO_3 in the iron hydroxide in the presence of PS-HSO_3 and PMG.

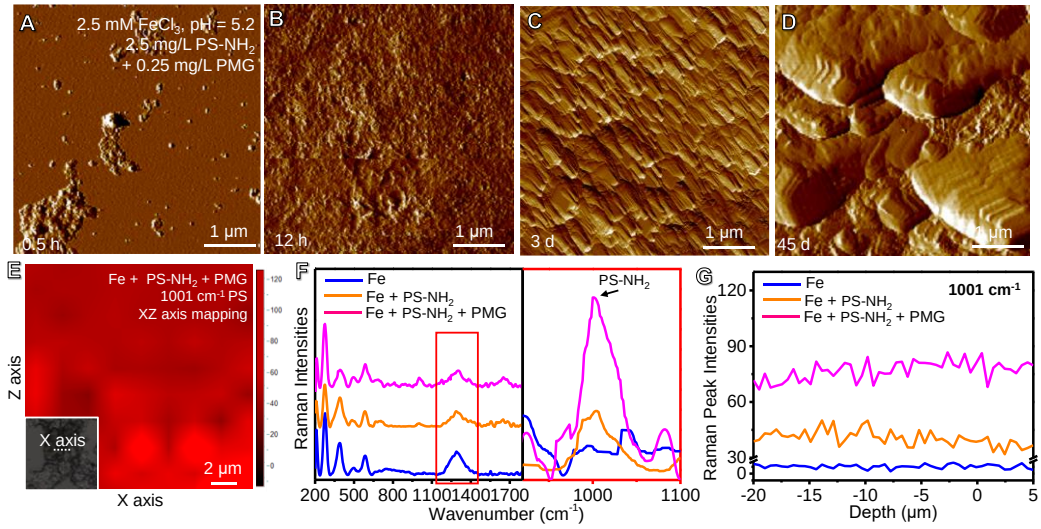

Figure S24. (A-D) Ex situ AFM deflection imaging of the crystallization and phase transformation process of iron hydroxide precipitates in solutions containing PS-NH_2 and PMG showing that certain crystalline faces appeared after 45 d of reactions. (E) Raman mapping (at 1001 cm^{-1}) of the XZ axis for the iron hydroxide precipitates containing PS-NH_2 and PMG after 120 h of reactions, indicating the PS-NH_2 was occluded within the crystals. (F) Raman spectra of the iron hydroxide in the absence and presence of 2.5 mg/L PS-NH_2 or mixed 2.5 mg/L PS-NH_2 and 0.25 mg/L PMG. The PS-NH_{23} signals were stronger for mixed PS-NH_2 and PMG than PS-NH_2 alone. (G) The z axis signal intensities (at 1001 cm^{-1}) of PS-NH_2 in the iron hydroxide in the presence of PS-NH_2 and PMG.

SI References

(1) J. R. Anema, A. G. Brollo, A. Felten and C. Bittencourt, Surface-enhanced Raman scattering from polystyrene on gold clusters, *J. Raman Spectrosc.*, 2010, **41**, 745-751.

(2) M. B. Hay and S. C. B. Myneni, Structural environments of carboxyl groups in natural organic molecules from terrestrial systems. part 1: infrared spectroscopy, *Geochim. Cosmochim Acta*, 2007, **71**, 3518-3532.

(3) E. Stewart James, Vibrational spectra of primary and secondary aliphatic amines, *J. Chem. Phys.*, 1959, **3***0*, 1259-1265.

(4) H. G. M. Edwards, D. R. Brown, J. A. Dale and S. Plant, Raman spectroscopy of sulfonated polystyrene resins, *Vib. Spectrosc.*, 2000, **24**, 213-224.

(5) A. Feis, C. Gellini, M. Ricci, L. Tognaccini, M. Becucci and G. Smulevich, Surface-enhanced Raman scattering of glyphosate on dispersed silver nanoparticles: A reinterpretation based on model molecules, *Vib. Spectrosc.*, 2020, **108**, 103061.

(6) L. Borromeo, U. Zimmermann, S. Andò, G. Coletti, D. Bersani, D. Basso, P. Gentile, B. Schulz and E. Garzanti, Raman spectroscopy as a tool for magnesium estimation in Mg-calcite, *J. Raman Spectrosc.*, **2017**, *48*, 983-992.

(7) D. de Wall and M. A. Legodi, The preparation of magnetite, goethite, hematite and maghemite of pigment quality from mill scale iron waste, *Dyes Pigments*, **2007**, *74*, 161-168.